THE JOURNAL OF PHYSICAL CHEMISTRY C
A JOURNAL OF THE AMERICAN CHEMICAL SOCIETY

pubs.acs.org/JPCC Article

Light Amplification Materials Based on Biopolymers Doped with Dye Molecules—Structural Insights from ^{15}N and ^{13}C Solid-State Dynamic Nuclear Polarization

Mark V. Höfler, Nicolai Hoinka, Timmy Schäfer, Marilia Horn, Fabien Aussenac, Thomas Fuhrmann-Lieker,* and Torsten Gutmann*

Cite This: https://doi.org/10.1021/acs.jpcc.1c06737 Read Online

ACCESS | Metrics & More | Article Recommendations | Supporting Information

ABSTRACT: ^{13}C and ^{15}N solid-state nuclear magnetic resonance (NMR) combined with dynamic nuclear polarization (DNP) is used to investigate the structure of dye-doped biopolymer-based materials that can be used in amplified spontaneous emission (ASE) experiments. By comparing calligraphic paper prepared from cellulose and scaffolds prepared from chitosan as substrates, differences in the interactions of the carrier material with the dye molecule Calcofluor White are obtained. These are most probably induced by structural changes of the carrier material due to its interaction with water forming hydrogen bonds. Such structural differences may explain the obtained variation of the emission wavelength of Calcofluor White doped on these substrates in ASE experiments.

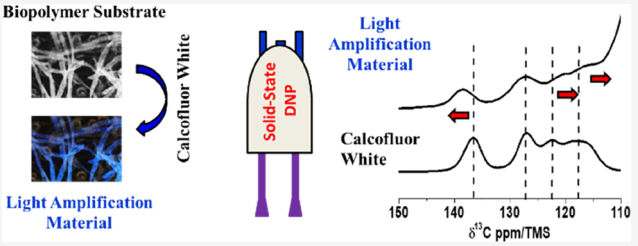

INTRODUCTION

In the past decades, paper substrates as well as chitosan and their derivatives have become the basis for a large variety of biocompatible functional materials with potential applications in different fields such as in food industry, drug delivery systems, or medical diagnostics.[1−8] More specific applications range from supporting materials for catalysts[9,10] and stimuli-responsive or sensoric molecules[11,12] over electronic and optical devices[13,14] to materials that have been recently used in amplified light emission experiments.[15,16] To make paper substrates or chitosan available, they have to be prepared from natural, renewable resources. For paper materials, typically cellulose fibers from plants are the basis for manufacturing.[17] Chitosan is prepared mainly by partial deacetylation of chitin from crustaceans, but can also be synthesized by certain fungi.[18] In the next step, the prepared carrier materials can be modified by molecules such as dyes that generate functionality. One possibility is the modification of the material by covalent grafting as it has been shown by Song at al.[19] for the fluorophore 1,8-naphthalimide and by some of us[20] for linking of rhodamine B on cellulose-derived materials, which can be both applied in sensorics. On the other hand, the molecules may also be adsorbed as shown for paper materials with application in gas sensing[21−23] or for chitosan, which was applied to adsorb dyes from waste water.[24]

As recently demonstrated by some of us,[15] conventional paper substrates can be simply treated with a fluorescent brightening agent (FBA) such as Calcofluor White and efficiently applied in amplified spontaneous emission (ASE) experiments. In this content, however, the following questions are still open: (i) How does the dye molecule interact with the supporting material. (ii) Are there differences between various carrier materials, i.e., paper substrate vs chitosan? Does the adsorption of the dye molecule on the carrier material induce structural changes? (iv) Does the use of different carrier materials influence the properties of amplified emission? To solve these quests, a detailed structural analysis has to be performed at a molecular level. This requires an appropriate analytical technique that allows the determination of local structures in these disordered solid materials.

Solid-state nuclear magnetic resonance (NMR) is a powerful technique that provides such information.[25] However, there are some limitations in terms of low intrinsic sensitivity for biopolymers that have only small surface areas, contain small amounts of surface molecules, or when nuclei such as ^{15}N have to be detected by solid-state NMR.[26−28] To overcome this disadvantage, it is necessary to boost the sensitivity which can be done by a combination of solid-state NMR with dynamic nuclear polarization (solid-state DNP).[29−34] This technique uses the polarization of unpaired electrons, which is 3 orders of magnitude higher and transfers it into nuclear polarization. Thus, the sensitivity of solid-state NMR is significantly

Received: July 29, 2021
Revised: September 11, 2021

enhanced as shown recently for a variety of cellulose-based materials.[20,35−40]

With the help of this technique, we wanted to identify the structural organization and interaction of dye molecules with the surface of the carrier material as well as the influence of solvents on the structure of the carrier materials. As model compounds, we used (i) a pure cellulose calligraphic paper and (ii) chitosan scaffolds as carrier materials, which were both impregnated with Calcofluor White.

The rest of this paper is organized as follows. After this brief Introduction section, the experimental details are given. This section is followed by the Results and Discussion section, where first the characterization of the two model systems with 1H → 13C and 1H → 15N CP MAS DNP is described and discussed in the context of structural changes of the carrier materials. Then, the results of the ASE experiments for the two model systems are presented and discussed in the context of structural differences.

METHODS

General. Calcofluor White (Fluorescent Brightener 28, sample **1**) was purchased from Sigma-Aldrich. Paper material (pure cellulose calligraphy paper, sample **2**) from Wenzhouh Halili Industry & Trade Co. (China) and chitosan scaffolds (sample **4**) were prepared from low-molecular-weight chitosan (sample **6**) purchased from Sigma-Aldrich. AMUPol was obtained from Cortecnet (France). Glycerol-d_8 and D_2O were purchased from Sigma-Aldrich and used without further purification. A list of all sample labels is given in Table 1. The detailed sample preparation is described in the following paragraphs.

Table 1. List of Sample Labels and Short Descriptions

sample Label	short description
sample **1**	Calcofluor White
sample **1a**	Calcofluor White + DNP juice
sample **2**	pure calligraphy paper
sample **2a**	pure calligraphy paper + DNP juice
sample **3**	calligraphy paper doped with Calcofluor White
sample **3a**	calligraphy paper doped with Calcofluor White + DNP juice
sample **4**	chitosan scaffolds
sample **4a**	chitosan scaffolds + DNP juice
sample **4b**	chitosan scaffolds + H_2O
sample **4c**	chitosan scaffolds + glycerol-d_8/D_2O/H_2O
sample **5**	chitosan scaffolds doped with Calcofluor White
sample **5a**	chitosan scaffolds doped with Calcofluor White + DNP juice
sample **5b**	chitosan scaffolds doped with Calcofluor White + H_2O
sample **5c**	chitosan scaffolds doped with Calcofluor White + glycerol-d_8/D_2O/H_2O
sample **6**	low-molecular-weight chitosan
sample **6b**	low-molecular-weight chitosan + H_2O
sample **6c**	low-molecular-weight chitosan + glycerol-d_8/D_2O/H_2O

General Sample Preparation. *Calligraphic Paper + Calcofluor White (Sample **3**).* In the first step, a solution of 1 mg/mL (ca. 1 mM) of Calcofluor White (sample **1**) (M = 960.95 g/mol) in demineralized water was prepared. The paper material (sample **2**) was then impregnated by dropping this solution with a pipette until complete wetting. The material was dried at room temperature, and the whole procedure was repeated one time to obtain sample **3**.

*Chitosan Scaffolds (Sample **4**).* In the first step, the acetylation degree of the low-molecular-weight chitosan from Sigma-Aldrich (15%) was determined by proton nuclear magnetic resonance spectroscopy (^{1}H NMR) according to the method developed and validated by Lavertu et al.[41] The molecular weight (120 kDa) was determined by the capillary viscometer procedure,[42] in which flow time measurements were performed on an Ubbelohde viscometer. A 1% (w/w) chitosan gel was prepared by dissolution of the polysaccharide in a 1% acetic acid (HAc) aqueous solution under stirring at room temperature for 24 h. After that, the solution was frozen in liquid nitrogen and freeze-dried to obtain the porous scaffold.

*Chitosan Scaffolds + Calcofluor White (Sample **5**).* The chitosan scaffolds were prepared as described above. A Calcofluor White solution of 1 mg/mL (ca. 1 mM) was used to impregnate the sample.

Sample Preparation for DNP NMR Experiments. *Calcofluor White for DNP (Sample **1a**).* As a reference, a blank sample of Calcofluor White was prepared for DNP (sample **1a**), for which 28.1 mg of Calcofluor White (sample **1**) was impregnated with 14 μL of a 15 mM AMUPol[43] solution in glycerol-d_8/D_2O/H_2O (60:30:10 w/w/w). The wetted sample was then packed into a 3.2 mm sapphire rotor, which was sealed with a Teflon plug and closed with a ZrO_2 driving cap.

*Calligraphic Paper for DNP (Sample **2a**).* In a similar way, a blank sample of the calligraphic paper was prepared for DNP (sample **2a**) employing 14 mg of the paper material (sample **2**) and 14 μL of the 15 mM AMUPol solution in glycerol-d_8/D_2O/H_2O (60:30:10 w/w/w).

*Calligraphic Paper + Calcofluor White for DNP (Sample **3a**).* With the dye-doped calligraphic paper, the DNP sample preparation was performed similarly to sample **2a**. Typically, 14 mg of sample **3** was impregnated with 14 μL of the 15 mM AMUPol solution in glycerol-d_8/D_2O/H_2O (60:30:10 w/w/w) to obtain sample **3a**.

*Chitosan Scaffolds for DNP (Sample **4a**).* Similar to sample **1a**, a blank sample of chitosan scaffolds was prepared for DNP (sample **4a**). Thereby, 17 mg of sample **4** was mixed with 17 μL of the 15 mM AMUPol solution in glycerol-d_8/D_2O/H_2O (60:30:10 w/w/w).

*Chitosan Scaffolds + Calcofluor White for DNP (Sample **5a**).* With the dye-doped chitosan scaffolds, the DNP sample preparation was performed similarly to sample **4a**. In this case, 15 mg of sample **5** was mixed with 15 μL of the 15 mM AMUPol solution in glycerol-d_8/D_2O/H_2O (60:30:10 w/w/w) to obtain sample **5a**.

DNP NMR Experiments. Solid-state DNP NMR spectra of samples **1a**, **2a**, and **3a** were recorded in Darmstadt on a Bruker Avance III 400 DNP spectrometer corresponding to frequencies of 400.02 MHz for ^{1}H, 100.59 MHz for ^{13}C, and 40.54 MHz for ^{15}N. This spectrometer is equipped with a 3.2 mm low-temperature H/X/Y triple-resonance probe and uses a 9.7 T Bruker gyrotron system that generates microwaves at a frequency of 263 GHz.

To obtain the optimum recycle delay for cross-polarization (CP MAS) experiments, ^{1}H saturation recovery experiments with microwave irradiation (mw on) were performed for all samples with a saturation pulse train of 20 using $\pi/2$ pulses of 2.3 μs length. Analysis of the built-up time T_B was performed with an exponential fit function.

https://doi.org/10.1021/acs.jpcc.1c06737
J. Phys. Chem. C XXXX, XXX, XXX−XXX

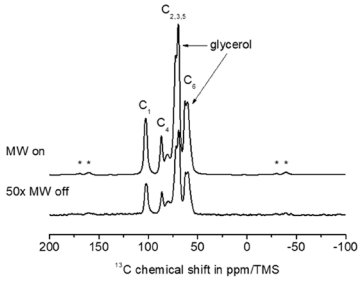

Chemical shift δ in ppm	Assignment
102.7	C_1
86.7	C_4 (cryst.)
80.6	C_4 (amorph)
77.0-65.5	glycerol + $C_{2,3,5}$
65.5-54.0	glycerol + C_6

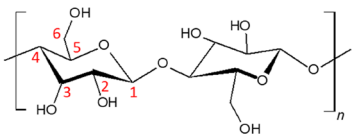

Figure 1. $^1H \rightarrow {}^{13}C$ CP MAS NMR spectra of calligraphic paper doped with Calcofluor White (sample **3a**) recorded with and without microwave irradiation (left) and their corresponding assignments (right). Note: Spectra were recorded at 10 kHz spinning. Spinning sidebands of glycerol are marked with asterisks.

$^1H \rightarrow {}^{13}C$ CP MAS experiments were recorded at 8 or 10 kHz spinning. A linear 100-50 ramp on ^1H was employed during contact. The contact time was set at 2 ms, and the recycle delay was set at $1.3 \cdot T_B$ (for T_B values, see Table S3). Each spectrum was recorded with 512 scans, and spinal64 decoupling[44] was applied during data acquisition. The chemical shift was referenced to TMS (0 ppm).

$^1H \rightarrow {}^{15}N$ CP MAS experiments were recorded at 10 kHz spinning. A linear 100-50 ramp on ^1H was employed during contact. The contact time was set at 3.5 ms, and the recycle delay was set at $1.3 \cdot T_B$ (for T_B values, see Table S3). The spectrum of sample **1a** was recorded with 1536 scans, and the spectrum of sample **3a** was recorded with 20 480 scans. For both samples, tppm decoupling[45] was applied during data acquisition. The chemical shift was referenced to liquid NH_3 (0 ppm) employing NH_4Cl (39.3 ppm) as external standard according to ref 46.

Solid-state DNP NMR spectra of samples **4a** and **5a** were recorded in Wissembourg (France) on a Bruker Avance NEO spectrometer with an Ascend 400 DNP magnet, corresponding to frequencies of 400.22 MHz for ^1H, 100.64 MHz for ^{13}C, and 40.55 MHz for ^{15}N. This spectrometer is equipped with a 3.2 mm low-temperature H/X/Y triple-resonance probe and a 4.8 T Bruker gyrotron system operating at second harmonics that generates microwaves at a frequency of 263 GHz.

To obtain the optimum recycle delay for cross-polarization (CP MAS) experiments, ^1H saturation recovery experiments with microwave irradiation (mw on) were performed for all samples with a saturation pulse train of 50 using $\pi/2$ pulses of 2.6 μs length. Analysis of the built-up time T_B was performed with an exponential fit function.

$^1H \rightarrow {}^{13}C$ CP MAS experiments were recorded at 8 or 10 kHz spinning. A linear 100-50 ramp on ^1H was employed during contact. The contact time was set at 2 ms, and the recycle delay was set at $1.3 \cdot T_B$ (for T_B values, see Table S3). Each spectrum was recorded with 512 scans, and spinal64 decoupling[44] was applied during data acquisition. The chemical shift was referenced to TMS using a silicone plug as an external standard (0 ppm).

$^1H \rightarrow {}^{15}N$ CP MAS experiments were recorded at 10 kHz spinning. A linear 100-50 ramp on ^1H was employed during contact. The contact time was set at 3.5 ms, and the recycle delay was set at $1.3 \cdot T_B$ (for T_B values, see Table S3). The spectra of samples **4a** and **5a** were each recorded with 16384 scans. For both samples, spinal64 decoupling[44] was applied during data acquisition. The chemical shift was referenced to liquid NH_3 (0 ppm) using glycine (30 ppm) as an external standard.

To obtain enhancement factors for the DNP spectra, the appropriate sample was measured with and without microwave irradiation. The factors were calculated by scaling the peak maxima to an equivalent value. The error was estimated by adding the percentage error of the noise level of both measurements. For large errors of about 100%, the enhancement is not defined (N/D).

Sample Preparation for Lasing Experiments. For both types of substrates, calligraphic paper and chitosan scaffolds, samples were prepared for optical amplification analysis. Similar to the general preparational steps, the substrates were impregnated with Calcofluor White (1 mg/mL) in demineralized water. After drying the samples, the process of wetting was repeated once.

ASE Experiments. For ASE experiments, a nitrogen laser (Laser Technik Berlin GmbH, MSG 800 SD) with a pulse duration shorter than 500 ps and a wavelength of λ = 337.1 nm was used as a source. Triggered single pulses with a fluence of 7815 $\mu J/cm^2$ were applied. To control the fluence of the incident light toward the sample, a neural density filter wheel (Thorlabs, NDC-50C 4M) was used. The input fluence was determined by averaging 100 pulses at a given set of neutral density (ND) filter setting and area of illumination. Laser Technik Berlin (LTB) provided a joule meter for the nitrogen laser. The sample of interest was fixed at a distance of 100 mm from the source. Sample translation to avoid depletion after a measurement is provided by an alignment stage (Newport ULTRAlign, Model 561D metric). To collect a sufficient amount of light, an optical fiber was placed in near-proximity to the illuminated area of the sample. Spectral analysis of the output light was performed by a detector array spectrometer (Avantes Starline "Avaspec 3648" with a spectral range from 300 to 820 nm and a resolution of 0.2 nm). Fluorescence experiments were performed on a Hitachi F-4500.

RESULTS AND DISCUSSION

$^1H \rightarrow {}^{13}C$ and $^1H \rightarrow {}^{15}N$ CP MAS DNP-Enhanced Solid-State NMR of Dye-Doped Paper Material. As a first model system, the calligraphic paper, which was doped with Calcofluor White (sample **3**), was investigated. This model system has been successfully applied previously in ASE experiments.[15] To study the interaction of the dye molecule

https://doi.org/10.1021/acs.jpcc.1c06737
J. Phys. Chem. C XXXX, XXX, XXX−XXX

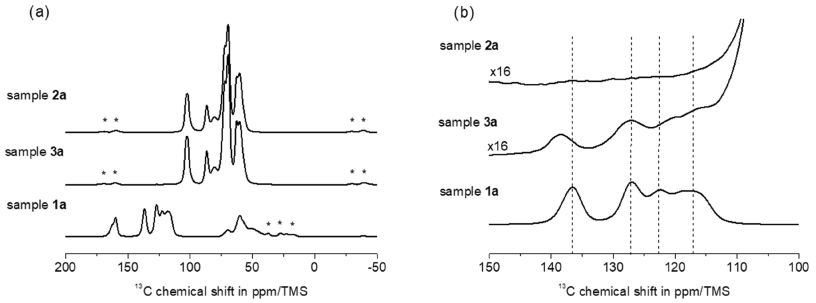

Figure 2. (a) DNP-enhanced $^{1}H \rightarrow {}^{13}C$ CP MAS NMR spectra of Calcofluor White (sample **1a**), calligraphic paper (sample **2a**), and calligraphic paper doped with Calcofluor White (sample **3a**). (b) Zoom in the spectral range between 100 and 150 ppm. Note: The scaling factors 16 were used to make signals of the Calcofluor White visible for sample **3a**. Spectra were recorded at 10 kHz spinning. Spinning sidebands are marked with asterisks. The dashed lines are used to guide the eye.

with the paper material in this model system, three different samples were prepared and inspected by DNP-enhanced ^{13}C and $^{1}H \rightarrow {}^{15}N$ CP MAS solid-state NMR, namely, the pure Calcofluor White dye (sample **1a**) as well as the pure calligraphic paper (sample **2a**) as references, and the calligraphic paper doped with Calcofluor White (sample **3a**).

For sample **3a**, the achievable DNP signal enhancement in $^{1}H \rightarrow {}^{13}C$ CP MAS NMR experiments was analyzed by comparing the spectra measured with and without microwave irradiation (Figure 1, left). The determination of the enhancement factors for each single signal (Table S1) shows that an enhancement up to 140 is reachable, which corresponds to a time saving factor of $140^2 = 19\,600$. As can be seen from Table S1, the enhancement factors of the signals obtained for sample **3a** are identical within the error margins with an average value of 123. This observation is a clear indication of a uniform transfer of the polarization through the sample. This result is not very surprising since the model system is homogeneously wetted and thus transfer via $^{1}H-{}^{1}H$ spin-diffusion through the sample is expected to be to the largest possible extent homogeneous.

To assign each signal in the spectrum of **3a**, it is necessary to compare this spectrum with reference spectra recorded for the neat substances, namely, Calcofluor White (sample **1a**) and pure calligraphic paper (sample **2a**). Thus, similar to sample **3a**, DNP-enhanced ^{13}C CP MAS NMR spectra for the reference samples **1a** and **2a** were recorded. To identify the isotropic signals in the DNP-enhanced $^{1}H \rightarrow {}^{13}C$ CP MAS spectra for each sample, they were recorded at two different spinning rates, at 8 and 10 kHz. The spectra obtained at different spinning rates for samples **1a** and **3a** are shown in Figure S1. For the isotropic signals obtained for Calcofluor White (sample **1a**), a clear signal assignment to functional groups is feasible by comparing with liquid NMR data. The full signal assignment is shown in Figure S2. With this in mind, the signal group at about 165 ppm in the $^{1}H \rightarrow {}^{13}C$ CP MAS spectrum of **1a** (Figure S1) is assigned to the carbon atoms of the 1,3,5-triazine ring of the dye molecule. Moreover, the signals at 50 ppm and 60 ppm are related to the CH_2 groups and the signals in the region between 115 and 145 ppm refer to the aromatic ring system present in the dye molecule.

Figure 2 shows the DNP-enhanced $^{1}H \rightarrow {}^{13}C$ CP MAS spectra of samples **1a** to **3a**. When comparing the spectral pattern obtained for calligraphic paper (sample **2a**) and calligraphic paper doped with Calcofluor White (sample **3a**) in Figure 2 (left), it is obvious that no significant difference between the two samples is observed. This is not very surprising since the amount of the dye molecule compared to the paper substrate is low. Enlargement of the spectral region between 100 and 150 ppm (Figure 2, right), however, shows that four additional signals with low intensities appeared at 138.5, 127.5, 120.5, and 116.0 ppm for sample **3a** compared to sample **2a**. These signals are assigned to small amounts of Calcofluor White molecules present in sample **3a**. Comparison of the chemical shifts obtained for the dye molecules in sample **3a** with the chemical shifts obtained for pure Calcofluor White (sample **1a**) shows significant deviations (see Table S4). While the signal at 138.5 ppm in the spectrum of sample **3a** is ~2 ppm low-field-shifted compared to sample **1a** (136.5 ppm), the signal at 127.5 ppm has the same shift in both samples and the signals at 120.5 ppm and 116.0 ppm in the spectrum of sample **3a** are ~2 ppm high-field-shifted compared to sample **1a** (122.5 and 118.0 ppm). These differences in chemical shifts clearly indicate the presence of interactions between the paper material and the dye molecule. It has to be noticed that this phenomenon may be also obtainable for the other signals of the dye molecule, which however are difficult to analyze since they overlay with signals of the cellulose or with spinning sidebands of the solvent matrix used for the DNP sample preparation. The second issue may be overcome by measuring the samples at higher spinning rates or using different solvent matrices, which is beyond the scope of the present work.

To shed more light on the interactions of the dye molecule with the paper substrate, DNP-enhanced $^{1}H \rightarrow {}^{15}N$ CP MAS spectra of the pure Calcofluor White (sample **1a**) and the calligraphic paper doped with Calcofluor White (sample **3a**) were recorded and are compared in Figure 3. A comparison of the chemical shift values is given in Table S5. The spectrum of pure Calcofluor White (sample **1a**) shows three signals, at 178.0, 112.5, and 91.5 ppm. The signal at 178.0 ppm, which contains a slightly high-field-shifted shoulder signal at 167.5 ppm, is clearly attributed to the three nitrogen atoms in the 1,3,5-triazine ring of Calcofluor White. The signals at 112.5 and 91.5 ppm are assigned to secondary and tertiary amine nitrogen atoms in different chemical environments. In contrast, the spectrum of the calligraphic paper doped with Calcofluor White (sample **3a**) shows only two signals, at 179.5 and 114.5 ppm. Furthermore, a weak signal almost at the noise level at about 94.5 ppm becomes visible. Compared with the signals obtained for **1a**, these signals differ in their intensity as well as in their chemical shifts depending on the functional group. While for the aromatic nitrogen atoms in the 1,3,5-triazine, the chemical shift difference is only moderate (less than 2 ppm), for the amine groups, it is significant (3–4 ppm). This

https://doi.org/10.1021/acs.jpcc.1c06737
J. Phys. Chem. C XXXX, XXX, XXX−XXX

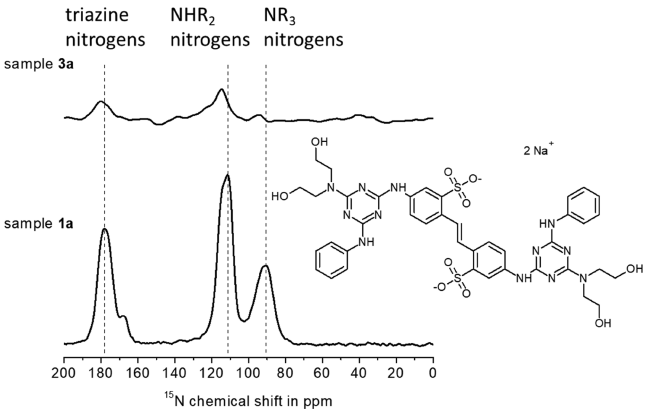

Figure 3. Comparison of DNP-enhanced $^{1}H \rightarrow {}^{15}N$ CP MAS NMR spectra of Calcofluor White (sample **1a**) and calligraphic paper doped with Calcofluor White (sample **3a**). Note: spectra were recorded at 10 kHz spinning.

indicates that the amine nitrogen atoms of the Calcofluor White molecule form H-bridges, which influence the chemical shift.

$^{1}H \rightarrow {}^{13}C$ and $^{1}H \rightarrow {}^{15}N$ CP MAS DNP-Enhanced Solid-State NMR of Dye-Doped Chitosan Scaffolds. To get deeper structural insights on the interactions of Calcofluor White with chitosan scaffolds, this material was also investigated with DNP-enhanced $^{1}H \rightarrow {}^{13}C$ and $^{1}H \rightarrow {}^{15}N$ CP MAS NMR. The chitosan scaffolds doped with Calcofluor White (sample **5a**) show enhancements of up to $\varepsilon = 71$ in the $^{1}H \rightarrow {}^{13}C$ CP MAS NMR, which is slightly lower than the enhancements obtained for the pure chitosan scaffolds (sample **4a**), which are up to $\varepsilon = 83$ (see Table S2 and Figure S4). Thereby, all peaks in the appropriate spectra show similar amplification within the error margins, which implies uniform distribution of polarization in the samples. This result is comparable with the result obtained for the calligraphic paper sample (see above).

The comparison of the $^{1}H \rightarrow {}^{13}C$ CP MAS DNP spectra of samples **4a**, **5a**, and **1a** is shown in Figure 4 (left). Both samples **4a** and **5a** show strong signals at ca. 60 and 72 ppm, which refer to glycerol used as a glass-forming agent in the DNP sample preparation. Next to these signals, two shoulder signals at about 55 and 80 ppm are visible, which are assigned to the C_2 and C_4 carbon atoms of glucosamine and N-acetylglucosamine moieties, respectively.[47,48] Furthermore, signals at 21.5, 172.5, and 179.5 ppm are obtained in the spectra. The signal at 21.5 ppm is typical for a methyl group and the signals at 172.5 and 179.5 ppm for carbonyl functions in different chemical environments and refer to N-acetylglucosamine moieties. These structure moieties are present in the scaffold samples next to glucosamine moieties, since they are manufactured from commercial chitosan (degree of acetylation 15%). According to Kameda et al.,[49] the latter signals do not refer to a $^{13}C-{}^{14}N$ coupling nor to crystalline and amorphous regions in the material. More probable, they occur due to the presence of different hydrogen-bond networks that effect the chemical shift of the carbonyl functions. The analysis of the area ratio of the signal at 179.5 ppm to the signal at 172.5 ppm (Figure 4 left, insets) only shows small changes from 65% for the scaffolds (sample **4a**) to 60% for the scaffolds doped with Calcofluor White (sample **5a**), which indicates that changes of the hydrogen-bond environments at the carbonyl function are only moderate when the scaffolds are doped with the dye molecules. Here, it has to be noticed that our semiquantitative analysis is based on the assumption that the cross-polarization efficiency is similar for both samples, which in first approximation should be valid for samples **4a** and **5a** containing similar sample composition. Furthermore, the DNP polarization transfer leading to the obtained signal intensities seems to be almost homogeneous as illustrated by the similar relative areas obtained for the signals in the spectra recorded with and without microwave irradiation (Figure S4).

The signals obtained at 101 and 96 ppm are assigned to C_1 of N-acetylglucosamine and glucosamine moieties in different hydrogen-bond environments.[50] Interestingly, by adding Calcofluor White (sample **5a**), the ratio of the signal at 96 ppm compared to the signal at 101 ppm changes strongly from 50% (sample **4a**) to 25% (sample **5a**) (Figure 4 left, insets). This change unlikely stems from TEMPO-mediated oxidation, which may take place due to the presence of TEMPO-derived radicals in the DNP matrix.[51] It is more probable that water or

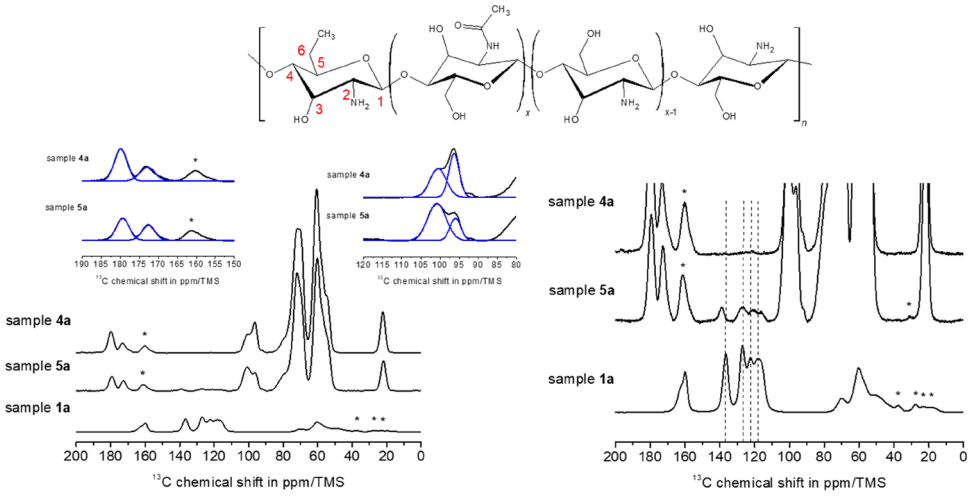

Figure 4. DNP-enhanced $^{1}H \rightarrow {}^{13}C$ CP MAS NMR spectra of Calcofluor White (sample **1a**), chitosan scaffolds (sample **4a**), and chitosan scaffolds doped with Calcofluor White (sample **5a**). Note: spectra were recorded at 10 kHz spinning. Spinning sidebands are marked with asterisks. For comparison, a spectrum of sample **5a** measured at 8 kHz is shown in Figure S3.

https://doi.org/10.1021/acs.jpcc.1c06737
J. Phys. Chem. C XXXX, XXX, XXX−XXX

glycerol-d_8/D_2O/H_2O used for the sample preparation affects this change.

To analyze the influence of the solvent on the structure of the material, solid-state NMR spectra of chitosan scaffolds and chitosan scaffolds doped with Calcofluor White as neat materials were recorded at room temperature, and compared to the spectra of these materials when wetted with water or with a mixture of glycerol-d_8/D_2O/H_2O (samples **4**, **4b**, **4c**, **5**, **5b**, **5c**). The spectra of chitosan scaffolds and these scaffolds doped with Calcofluor White (samples **4** and **5** in Figure S5) both show a broad signal composed of two subsignals centered at 102 and 99 ppm referring to C_1 of N-acetylglucosamine and glucosamine moieties in different hydrogen-bond environments. Furthermore, three signals in the carbonyl region are obtained for sample **4** (179.5, 176.0, 173.5 ppm), while only two are obtained for sample **5** (179.5, 173.5 ppm). By adding the glycerol-d_8/D_2O/H_2O matrix (samples **4c** and **5c**), the relative intensity of the signal of the carbonyl group at 173.5 ppm increases compared to the signal at 179.5 ppm. This trend gets even stronger when only water is added to the neat materials (samples **4b** and **5b**). For these samples in the carbonyl region, only one signal is left at 173.5 ppm.

One possible explanation refers to the theoretical work by Kameda and co-workers[52] who proposed that in peptide C═O, the isotropic carbon chemical shifts move to lower field with increasing strength of hydrogen bonds. By adding water to sample **4** or **5**, the materials swell (samples **4b** and **5b**) probably due to the semicrystalline nature of the biopolymer. Thus, the hydrogen bonds in the biopolymer become weaker or even broken. This would induce a decrease of the low-field carbonyl signal in the spectrum. The samples **4c** and **5c** then represent an intermediate step between the neat sample **4** or **5** and the samples prepared with water (samples **4b**, **5b**). Due to the presence of glycerol and only a small amount of water in the matrix, the effect on the strength of hydrogen bonds is less pronounced compared to pure water as a solvent. Thus, for samples **4b** and **5b**, a tiny signal at 179.5 ppm is still visible.

An analogous behavior is found for the C_1 signals. In the neat samples **4** and **5** (Figure S5), two signals are visible, one at 102 ppm and the second one occurring as a shoulder at about 99 ppm. By adding the glycerol-d_8/D_2O/H_2O matrix (samples **4c** and **5c**), only minor changes are observable. Adding pure water instead of the glycerol-d_8/D_2O/H_2O matrix, the observed effect gets more pronounced. The relative intensity of the signal at 99 ppm increases compared to the signal at 102 ppm. This observation is in agreement with the signal changes in the carbonyl region explained earlier and is assumed to refer to the change of the strength of the hydrogen-bond network in close vicinity to the C_1 carbon atoms in the materials.

Interestingly, the observations described above are not found for a chitosan sample (sample **6**) as received from Sigma-Aldrich. In Figure S6, the spectra of this sample impregnated with water (sample **6a**) and with a glycerol-d_8/D_2O/H_2O matrix (sample **6b**) are shown. In the carbonyl region, only one signal at 174 ppm is visible and also the signal at 105 ppm does not show two peaks. This is valid for samples **6**, **6a** and **6b**. One possible explanation refers to the presence of strong electrostatic interactions in the chitosan sample, which may prevent this sample to swell upon reaction with water. Such interactions are known for chitosan as a plasticizer effect when, for example, small amounts of glycerol react with chitosan.[53−55] For the chitosan scaffolds (sample **4**) which were prepared under acidic conditions, it seems that this effect has vanished and thus swelling of the material upon treatment with solvents/doping with Calcofluor White is induced.

Similarly, the structure of the paper-based samples **2** and **3** is not affected by the solvent matrix. As shown in Figure S7, when paper substrates are impregnated with different matrices, the C_1 signal of the cellulose is always accessible and shows no significant difference when compared for different matrices.

Next to the already described signals visible in **4a** and **5a**, additional signals with low intensity have appeared for sample **5a**. By enlarging the spectra (Figure 4 right), signals at 139.0, 127.0, 121.0, and 116.5 ppm are clearly identified. These peaks refer to the dye molecule. To guarantee consistency, all spectra were referenced on the low-field glycerol signal at 60 ppm. This reference points out a shift of the pure dye molecule in glycerol-d_8/D_2O/H_2O matrix (sample **1a**) compared to the chitosan scaffolds doped with the dye molecule (sample **5a**) approximately by the same values obtained for the paper sample doped with dye molecules (sample **2a**). By changing the spinning frequency from 10 to 8 kHz (Figure S3), another peak at about 162 ppm becomes visible. This peak is again low-field-shifted by 2 ppm in comparison to the pure dye molecule glycerol-d_8/D_2O/H_2O matrix (sample **1a**).

Since chitosan has an additional NH_2 group compared to cellulose, it is even more likely to record $^1H \rightarrow {}^{15}N$ CP MAS spectra. In Figure 5, the comparison between the $^1H \rightarrow {}^{15}N$ CP MAS spectra of Calcofluor White (sample **1a**), chitosan scaffolds (sample **4a**), and chitosan scaffolds doped with Calcofluor White (sample **5a**) is displayed. In sample **4a**, three signals are visible. The signal at 125.5 ppm is attributed to the N-acetylglycosamine moieties. The two peaks at 33 and 25 ppm indicate amine groups in glycosamine moieties.[56] The separation of these signals is most probably related to the protonation state of the amine groups, which strongly acts on the ^{15}N chemical shift. Based on refs 57, 58, the signals at 33 and 25 ppm may refer to NH_3^+ and NH_2 groups, respectively. Note that in the work by Dos et al.,[57] the ^{15}N spectra are referenced to NH_4Cl (0 ppm), while in the present work, they are referenced to NH_4Cl (39.3 ppm). The most pronounced effect in the $^1H \rightarrow {}^{15}N$ CP MAS spectra of samples **4a** and **5a** in Figure 5 is the change of the relative intensities of the peaks at 33 and 25 ppm, which has strongly decreased for sample **5a**

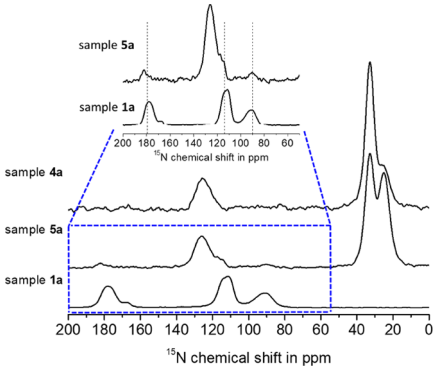

Figure 5. DNP-enhanced $^1H \rightarrow {}^{15}N$ CP MAS NMR spectra of Calcofluor White (sample **1a**), chitosan scaffolds (sample **4a**), and chitosan scaffolds doped with Calcofluor White (sample **5a**). Note: spectra were recorded at 10 kHz spinning. The inset shows the enlarged spectrum of sample **5a** together with the spectrum of sample **1a** in the range of 50−200 ppm to make the signals of the dye visible in sample **5a**. The dashed lines in this inset are used to guide the eye.

https://doi.org/10.1021/acs.jpcc.1c06737
J. Phys. Chem. C XXXX, XXX, XXX−XXX

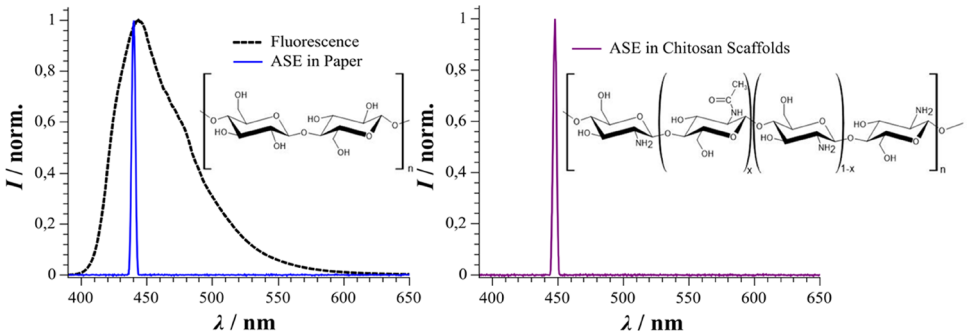

Figure 6. Left: ASE experiment performed on calligraphic paper doped with Calcofluor White (sample **3**) and fluorescence spectrum of sample **3**. Right: ASE experiment performed on chitosan scaffolds doped with Calcofluor White (sample **5**). Note: The maximum intensity of the spectra was normalized to 1. The insets show a cut of the structure of the appropriate carrier material (paper and chitosan scaffolds).

compared to sample **4a**. The amount of water used in the sample preparations seems to be responsible for this observation, since it can affect the protonation state of the amine groups and thus the ratio between NH_3^+ and NH_2 groups. Additionally, signals at 180.5, 116.5, and 90.5 ppm occur in the spectra of sample **5a**. These are assigned to Calcofluor White. Compared to the spectrum of neat Calcofluor White (sample **1a**), where signals are obtained at 178, 112.5, and 91.5 ppm, these signals are shifted by a few ppm, indicating an interaction of the Calcofluor White with the chitosan scaffold via hydrogen bonds, which induce a change of the ^{15}N chemical shift. This observation is in agreement with the changes obtained for Calcofluor White doped on calligraphic paper described in the last section.

Applications of Dye-Doped Paper and Dye-Doped Chitosan Scaffolds. Finally, ASE experiments were performed on calligraphic paper doped with Calcofluor White (sample **3**) and chitosan scaffolds doped with Calcofluor White (sample **5**) to compare their light emission behavior. From these experiments (Figure 6), a single emission line with a narrow FWHM of 3 nm was found for both materials. This observation is expected and demonstrates the functionality of these two samples as ASE substrates. More interestingly, for the calligraphic paper doped with Calcofluor White (sample **3**), the emission line is centered at 440 nm, while for the chitosan scaffolds doped with Calcofluor White (sample **5**), it is centered at 448 nm, although both samples contain the same dye molecule, namely, Calcofluor White.

These obtained different emission wavelengths are most probably induced by the interaction of the dye molecule with the carrier material for which hydrogen bonds seem to play a key role as described in the previous sections. The ability of the paper substrate to form hydrogen-bond networks is significantly different from that of the chitosan scaffolds. Next to these hydrogen bonds, however, also electrostatic interactions have to be taken into account. Since Calcofluor White is an anionic dye, a favored interaction of the sulfonate group with the amino groups of glucosamine moieties is expected. Such an interaction is less feasible for the calligraphic paper, which contains mainly cellobiose moieties. Thus, the significant difference in the wavelength of the emitted light may be explained.

CONCLUSIONS

In conclusion, using DNP-enhanced ^{13}C and ^{15}N solid-state NMR spectroscopy, it was possible to show that the dye molecule, namely, Calcofluor White, interacts with carrier materials based on biopolymers in a different manner. Here, possible interactions of water with the carrier material upon sample preparation play a key role. In detail, by comparing the NMR spectra of chitosan scaffolds with the one doped with Calcofluor White, significant structural changes were found for the chemical environment of C_1 in glucosamine and N-acetylglycosamine moieties. This was not explicitly found for the calligraphic paper as the carrier material where structural changes due to sample preparation with water can be neglected.

In ASE experiments, both materials reveal a very narrow FWHM of 3 nm, but an 8 nm redshift of the peak center is obtained for chitosan scaffolds doped with Calcofluor White compared to calligraphic paper doped with Calcofluor White. This demonstrates that the interactions of the dye molecule with the carrier material in combination with structural changes, which depend on the carrier material, play a key role to understand their optical properties in ASE experiments.

ASSOCIATED CONTENT

Supporting Information

The Supporting Information is available free of charge at https://pubs.acs.org/doi/10.1021/acs.jpcc.1c06737.

Signal assignments and enhancements of specific signals, ^1H built-up times T_B, ^{13}C and ^{15}N chemical shifts obtained for different samples, ^{13}C solution NMR spectrum of Calcofluor White with signal assignment, DNP-enhanced ^{13}C CP MAS spectra of samples recorded at different spinning rates, standard ^{13}C CP MAS solid-state NMR spectra of different materials with various sample preparations, and experimental details of standard solid-state NMR experiments (PDF)

AUTHOR INFORMATION

Corresponding Authors

Thomas Fuhrmann-Lieker − *Macromolecular Chemistry and Molecular Materials, Center of Interdisciplinary Nanostructure Science and Technology, Universität Kassel, D-34132 Kassel, Germany;* orcid.org/0000-0003-3473-534X; Email: th.fuhrmann@uni-kassel.de

Torsten Gutmann − *Institute of Inorganic and Physical Chemistry, Technische Universität Darmstadt, D-64287 Darmstadt, Germany;* orcid.org/0000-0001-6214-2272; Email: gutmann@chemie.tu-darmstadt.de

https://doi.org/10.1021/acs.jpcc.1c06737
J. Phys. Chem. C XXXX, XXX, XXX−XXX

Authors

Mark V. Höfler − *Institute of Inorganic and Physical Chemistry, Technische Universität Darmstadt, D-64287 Darmstadt, Germany*

Nicolai Hoinka − *Macromolecular Chemistry and Molecular Materials, Center of Interdisciplinary Nanostructure Science and Technology, Universität Kassel, D-34132 Kassel, Germany; German Research Center for Environmental Health (HMGU), Helmholtz Zentrum München, D-85764 Neuherberg, Germany*

Timmy Schäfer − *Institute of Inorganic and Physical Chemistry, Technische Universität Darmstadt, D-64287 Darmstadt, Germany*

Marilia Horn − *Macromolecular Chemistry and Molecular Materials, Center of Interdisciplinary Nanostructure Science and Technology, Universität Kassel, D-34132 Kassel, Germany*

Fabien Aussenac − *Bruker France SAS, F-67160 Wissembourg, France*

Complete contact information is available at: https://pubs.acs.org/10.1021/acs.jpcc.1c06737

Notes

The authors declare no competing financial interest.

■ ACKNOWLEDGMENTS

This work was supported by the DFG under contract GU-1650/3-1. The authors thank Prof. Buntkowsky as well as Bruker Biospin for the generous allocation of measurement time at their 400 MHz DNP spectrometers in Darmstadt and Wissembourg.

■ REFERENCES

(1) Ahmed, S.; Ikram, S. Chitosan & Its Derivatives: A Review in Recent Innovations. *Int. J. Pharm. Sci. Res.* **2015**, *6*, 14−30.

(2) Wang, W. J.; Xue, C. H.; Mao, X. Z. Chitosan: Structural Modification, Biological Activity and Application. *Int. J. Biol. Macromol.* **2020**, *164*, 4532−4546.

(3) Kumar, A. A.; Hennek, J. W.; Smith, B. S.; Kumar, S.; Beattie, P.; Jain, S.; Rolland, J. P.; Stossel, T. P.; Chunda-Liyoka, C.; Whitesides, G. M. From the Bench to the Field in Low-Cost Diagnostics: Two Case Studies. *Angew. Chem., Int. Ed.* **2015**, *54*, 5836−5853.

(4) Ravi Kumar, M. N. V. A Review of Chitin and Chitosan Applications. *React. Funct. Polym.* **2000**, *46*, 1−27.

(5) Martinez, A. W.; Phillips, S. T.; Whitesides, G. M.; Carrilho, E. Diagnostics for the Developing World: Microfluidic Paper-Based Analytical Devices. *Anal. Chem.* **2010**, *82*, 3−10.

(6) Qi, J.; Fan, X.-X.; Deng, D.-M.; He, H.-B.; Luo, L.-Q. Progress in Rapid Detection Techniques Using Paper-Based Platforms for Food Safety. *Chin. J. Anal. Chem.* **2020**, *48*, 1616−1624.

(7) Morin-Crini, N.; Lichtfouse, E.; Torri, G.; Crini, G. Applications of Chitosan in Food, Pharmaceuticals, Medicine, Cosmetics, Agriculture, Textiles, Pulp and Paper, Biotechnology, and Environmental Chemistry. *Environ. Chem. Lett.* **2019**, *17*, 1667−1692.

(8) Xia, Y. Y.; Si, J.; Li, Z. Y. Fabrication Techniques for Microfluidic Paper-Based Analytical Devices and Their Applications for Biological Testing: A Review. *Biosens. Bioelectron.* **2016**, *77*, 774−789.

(9) Krajewska, B. Application of Chitin- and Chitosan-Based Materials for Enzyme Immobilizations: A Review. *Enzyme Microb. Technol.* **2004**, *35*, 126−139.

(10) Macquarrie, D. J.; Hardy, J. J. E. Applications of Functionalized Chitosan in Catalysis. *Ind. Eng. Chem. Res.* **2005**, *44*, 8499−8520.

(11) Li, Z. J.; Yang, X. H.; Li, W.; Liu, H. B. Stimuli-Responsive Cellulose Paper Materials. *Carbohydr. Polym.* **2019**, *210*, 350−363.

(12) Mahadeva, S. K.; Walus, K.; Stoeber, B. Paper as a Platform for Sensing Applications and Other Devices: A Review. *ACS Appl. Mater. Interfaces* **2015**, *7*, 8345−8362.

(13) Lee, C.; Kim, S.; Cho, Y. H. Silk and Paper: Progress and Prospects in Green Photonics and Electronics. *Adv. Sustainable Syst.* **2020**, *9*, No. 2000216.

(14) Lin, Y.; Gritsenko, D.; Liu, Q.; Lu, X. N.; Xu, J. Recent Advancements in Functionalized Paper-Based Electronics. *ACS Appl. Mater. Interfaces* **2016**, *8*, 20501−20515.

(15) Hoinka, N. M.; Fuhrmann-Lieker, T. Amplified Spontaneous Emission in Paper. *Sci. Rep.* **2019**, *9*, No. 1862.

(16) Viola, I.; Ghofraniha, N.; Zacheo, A.; Arima, V.; Conti, C.; Gigli, G. Random Laser Emission from a Paper-Based Device. *J. Mater. Chem. C* **2013**, *1*, 8128−8133.

(17) Blechschmidt, J. *Taschenbuch Der Papiertechnik*; Carl Hanser Verlag: München, 2013; Vol. *2*.

(18) Gadgey, K. K.; Bahekar, A. Studies on Extraction Methods of Chitin from Crab Shell and Investigation of Its Mechanical Properties. *Int. J. Mech. Eng. Technol.* **2017**, *8*, 220−231.

(19) Song, R. Y.; Zhang, Q.; Chu, Y. L.; Zhang, L.; Dai, H. Q.; Wu, W. B. Fluorescent Cellulose Nanocrystals for the Detection of Lead Ions in Complete Aqueous Solution. *Cellulose* **2019**, *26*, 9553−9565.

(20) Zhao, L.; Li, W.; Plog, A.; Xu, Y.; Buntkowsky, G.; Gutmann, T.; Zhang, K. Multi-Responsive Cellulose Nanocrystal-Rhodamine Conjugates: An Advanced Structure Study by Solid-State Dynamic Nuclear Polarization (DNP) NMR. *Phys. Chem. Chem. Phys.* **2014**, *16*, 26322−26329.

(21) Kos, P.; Plenio, H. A Fluorescent Molecular Probe for the Detection of Hydrogen Based on Oxidative Addition Reactions with Crabtree-Type Hydrogenation Catalysts. *Angew. Chem., Int. Ed.* **2015**, *54*, 13293−13296.

(22) Bergmann, M.; Plenio, H. Giving an Odor to Carbon Monoxide: Malodorogenic Sensing of Carbon Monoxide Via Ircl(Cod)(Nhc) Complexes. *Eur. J. Inorg. Chem.* **2018**, *2018*, 2054−2059.

(23) Halter, O.; Plenio, H. Fluorescent Dyes in Organometallic Chemistry: Coumarin-Tagged Nhc-Metal Complexes. *Eur. J. Inorg. Chem.* **2018**, *2018*, 2935−2943.

(24) Kyzas, G. Z.; Bikiaris, D. N. Recent Modifications of Chitosan for Adsorption Applications: A Critical and Systematic Review. *Mar. Drugs* **2015**, *13*, 312−337.

(25) Moran, R. F.; Dawson, D. M.; Ashbrook, S. E. Exploiting NMR Spectroscopy for the Study of Disorder in Solids. *Int. Rev. Phys. Chem.* **2017**, *36*, 39−115.

(26) Gutmann, T.; Kumari, B.; Zhao, L.; Breitzke, H.; Schöttner, S.; Rüttiger, C.; Gallei, M. Dynamic Nuclear Polarization Signal Amplification as a Sensitive Probe for Specific Functionalization of Complex Paper Substrates. *J. Phys. Chem. C* **2017**, *121*, 3896−3903.

(27) Liu, P.; Liu, H.; Schäfer, T.; Gutmann, T.; Gibhardt, H.; Qi, H.; Tian, L.; Zhang, X.; Buntkowsky, G.; Zhang, K. Unexpected Selective Alkaline Periodate Oxidation of Chitin for the Isolation of Chitin Nanocrystals. *Green Chem.* **2021**, *23*, 745−751.

(28) Zhao, W. C.; Fernando, L. D.; Kirui, A.; Deligey, F.; Wang, T. Solid-State NMR of Plant and Fungal Cell Walls: A Critical Review. *Solid State Nucl. Magn. Reson.* **2020**, *107*, No. 101660.

(29) Akbey, Ü.; Franks, W. T.; Linden, A.; Orwick-Rydmark, M.; Lange, S.; Oschkinat, H. Dynamic Nuclear Polarization Enhanced NMR in the Solid-State. In *Hyperpolarization Methods in NMR Spectroscopy*; Springer: Berlin, 2013; Vol. *338*, pp 181−228.

(30) Barnes, A. B.; De Paepe, G.; van der Wel, P. C. A.; Hu, K. N.; Joo, C. G.; Bajaj, V. S.; Mak-Jurkauskas, M. L.; Sirigiri, J. R.; Herzfeld, J.; Temkin, R. J.; et al. High-Field Dynamic Nuclear Polarization for Solid and Solution Biological NMR. *Appl. Magn. Reson.* **2008**, *34*, 237−263.

(31) Gutmann, T.; Buntkowsky, G. Solid-State NMR Studies of Supported Transition Metal Catalysts and Nanoparticles. In *Modern Magnetic Resonance*; Springer International Publishing: Cham, 2017; pp 1−21.

(32) Gutmann, T.; Groszewicz, P. B.; Buntkowsky, G. Solid-State NMR of Nanocrystals. *Annu. Rep. NMR Spectrosc.* **2019**, *97*, 1−82.
(33) Rankin, A. G. M.; Trebosc, J.; Pourpoint, F.; Amoureux, J. P.; Lafon, O. Recent Developments in MAS DNP-NMR of Materials. *Solid State Nucl. Magn. Reson.* **2019**, *101*, 116−143.
(34) Thankamony, A. S. L.; Wittmann, J. J.; Kaushik, M.; Corzilius, B. Dynamic Nuclear Polarization for Sensitivity Enhancement in Modern Solid-State NMR. *Prog. Nucl. Magn. Reson. Spectrosc.* **2017**, *102*−*103*, 120−195.
(35) Perras, F. A.; Luo, H.; Zhang, X. M.; Mosier, N. S.; Pruski, M.; Abu-Omar, M. M. Atomic-Level Structure Characterization of Biomass Pre- and Post-Lignin Treatment by Dynamic Nuclear Polarization-Enhanced Solid-State NMR. *J. Phys. Chem. A* **2017**, *121*, 623−630.
(36) Takahashi, H.; Lee, D.; Dubois, L.; Bardet, M.; Hediger, S.; De Paepe, G. Rapid Natural-Abundance 2D C-13-C-13 Correlation Spectroscopy Using Dynamic Nuclear Polarization Enhanced Solid-State NMR and Matrix-Free Sample Preparation. *Angew. Chem., Int. Ed.* **2012**, *51*, 11766−11769.
(37) Kumar, A.; Durand, H.; Zeno, E.; Balsollier, C.; Watbled, B.; Sillard, C.; Fort, S.; Baussanne, I.; Belgacem, N.; Lee, D.; et al. The Surface Chemistry of a Nanocellulose Drug Carrier Unravelled by MAS-DNP. *Chem. Sci.* **2020**, *11*, 3868−3877.
(38) Zhao, L.; Smolarkiewicz, I.; Limbach, H. H.; Breitzke, H.; Pogorzelec-Glaser, K.; Pankiewicz, R.; Tritt-Goc, J.; Gutmann, T.; Buntkowsky, G. Imidazole-Doped Cellulose as Membrane for Fuel Cells: Structural and Dynamic Insights from Solid-State NMR. *J. Phys. Chem. C* **2016**, *120*, 19574−19585.
(39) Groszewicz, P. B.; Mendes, P.; Kumari, B.; Lins, J.; Biesalski, M.; Gutmann, T.; Buntkowsky, G. N-Hydroxysuccinimide-Activated Esters as a Functionalization Agent for Amino Cellulose: Synthesis and Solid-State NMR Characterization. *Cellulose* **2020**, *27*, 1239−1254.
(40) Wang, T.; Park, Y. B.; Caporini, M. A.; Rosay, M.; Zhong, L. H.; Cosgrove, D. J.; Hong, M. Sensitivity-Enhanced Solid-State NMR Detection of Expansin's Target in Plant Cell Walls. *Proc. Natl. Acad. Sci. U.S.A.* **2013**, *110*, 16444−16449.
(41) Lavertu, M.; Xia, Z.; Serreqi, A. N.; Berrada, M.; Rodrigues, A.; Wang, D.; Buschmann, M. D.; Gupta, A. A Validated 1H NMR Method for the Determination of the Degree of Deacetylation of Chitosan. *J. Pharm. Biomed. Anal.* **2003**, *32*, 1149−1158.
(42) Rinaudo, M. Chitin and Chitosan: Properties and Applications. *Prog. Polym. Sci.* **2006**, *31*, 603−632.
(43) Sauvée, C.; Rosay, M.; Casano, G.; Aussenac, F.; Weber, R. T.; Ouari, O.; Tordo, P. Highly Efficient, Water-Soluble Polarizing Agents for Dynamic Nuclear Polarization at High Frequency. *Angew. Chem., Int. Ed.* **2013**, *52*, 10858−10861.
(44) Fung, B. M.; Khitrin, A. K.; Ermolaev, K. An Improved Broadband Decoupling Sequence for Liquid Crystals and Solids. *J. Magn. Reson.* **2000**, *142*, 97−101.
(45) Bennett, A. E.; Rienstra, C. M.; Auger, M.; Lakshmi, K. V.; Griffin, R. G. Heteronuclear Decoupling in Rotating Solids. *J. Chem. Phys.* **1995**, *103*, 6951−6958.
(46) Bertani, P.; Raya, J.; Bechinger, B. 15n Chemical Shift Referencing in Solid State NMR. *Solid State Nucl. Magn. Reson.* **2014**, *61*−*62*, 15−18.
(47) Kasaai, M. R. Determination of the Degree of N-Acetylation for Chitin and Chitosan by Various NMR Spectroscopy Techniques: A Review. *Carbohydr. Polym.* **2010**, *79*, 801−810.
(48) Tanner, S. F.; Chanzy, H.; Vincendon, M.; Roux, J. C.; Gaill, F. High-Resolution Solid-State Carbon-13 Nuclear Magnetic Resonance Study of Chitin. *Macromolecules* **1990**, *23*, 3576−3583.
(49) Kameda, T.; Miyazawa, M.; Ono, H.; Yoshida, M. Hydrogen Bonding Structure and Stability of A-Chitin Studied by 13C Solid-State NMR. *Macromol. Biosci.* **2005**, *5*, 103−106.
(50) Saito, H.; Tabeta, R.; Ogawa, K. High-Resolution Solid-State Carbon-13 NMR Study of Chitosan and Its Salts with Acids: Conformational Characterization of Polymorphs and Helical Structures as Viewed from the Conformation-Dependent Carbon-13 Chemical Shifts. *Macromolecules* **1987**, *20*, 2424−2430.
(51) Fan, Y.; Saito, T.; Isogai, A. Tempo-Mediated Oxidation of B-Chitin to Prepare Individual Nanofibrils. *Carbohydr. Polym.* **2009**, *77*, 832−838.
(52) Kameda, T.; Takeda, N.; Kuroki, S.; Kurosu, H.; Ando, S.; Ando, I.; Shoji, A.; Ozaki, T. Hydrogen-Bonded Structure and C-13 NMR Chemical Shift Tensor of Amino Acid Residue Carbonyl Carbons of Peptides and Polypeptides in the Crystalline State. *J. Mol. Struct.* **1996**, *384*, 17−23.
(53) Rodríguez-Núñez, J. R.; Madera-Santana, T. J.; Sánchez-Machado, D. I.; López-Cervantes, J.; Soto Valdez, H. Chitosan/Hydrophilic Plasticizer-Based Films: Preparation, Physicochemical and Antimicrobial Properties. *J. Polym. Environ.* **2014**, *22*, 41−51.
(54) Chen, M. J.; Runge, T.; Wang, L. L.; Li, R. M.; Feng, J.; Shu, X. L.; Shi, Q. S. Hydrogen Bonding Impact on Chitosan Plasticization. *Carbohydr. Polym.* **2018**, *200*, 115−121.
(55) Domján, A.; Bajdik, J.; Pintye-Hodi, K. Understanding of the Plasticizing Effects of Glycerol and Peg 400 on Chitosan Films Using Solid-State NMR Spectroscopy. *Macromolecules* **2009**, *42*, 4667−4673.
(56) Heux, L.; Brugnerotto, J.; Desbrières, J.; Versali, M. F.; Rinaudo, M. Solid State NMR for Determination of Degree of Acetylation of Chitin and Chitosan. *Biomacromolecules* **2000**, *1*, 746−751.
(57) Dos, A.; Schimming, V.; Chan-Huot, M.; Limbach, H. H. Effects of Hydration on the Acid-Base Interactions and Secondary Structures of Poly-L-Lysine Probed by N-15 and C-13 Solid State NMR. *Phys. Chem. Chem. Phys.* **2010**, *12*, 10235−10245.
(58) Gartner, C.; López, B. L.; Sierra, L.; Graf, R.; Spiess, H. W.; Gaborieau, M. Interplay between Structure and Dynamics in Chitosan Films Investigated with Solid-State NMR, Dynamic Mechanical Analysis, and X-Ray Diffraction. *Biomacromolecules* **2011**, *12*, 1380−1386.

https://doi.org/10.1021/acs.jpcc.1c06737
J. Phys. Chem. C XXXX, XXX, XXX−XXX